Fabrication of High-active Phosphatases-like Fluorescent Cerium-doped Carbon Dots for In-situ Monitoring Hydrolysis of Phosphate Diester

Jinyan Du*, Shuangqing Qi, Juan Chen, Ying Yang, Tingting Fan, Ping Zhang, Shujuan Zhuo, Changqing Zhu*

Anhui Key Laboratory of Chemo-Biosensing, Key Laboratory of Functional Molecular Solids, Ministry of Education, College of Chemistry and Materials Science, Anhui Normal University, Wuhu, 241000, PR China.

*Corresponding authors, E-mail addresses: dujinyn@mail.ahnu.edu.cn (J. Y. Du), zhucq@mail.ahnu.edu.cn (C. Q. Zhu).

Degradation of pesticide

1. Stock standard solutions

Individual stock standard solution (ca.1000 mg/L) of pesticides was prepared by dissolving 25 mg chlorpyrifos in 25 mL of acetone. All standard solutions were stored in glass-stoppered flasks at 4℃.

2. Pretreatment

In a typical experiment, 1.0 ml stock solution of chlorpyrifos and 1.0 ml CeCDs were introduced into a colorimetric tube. At 25 ℃ and pH 8.8, the reaction liquid was shaked for 48 h, then processed according to the GB/T 5009. 145-2003 for determination of chlorpyrifos degradation through GC-MS.

The former sample pretreatment: 3 mL mixture was taken after biodegradation reaction, and extracted by adding 10 mL ethyl acetate. Therein 5 ml of the organic phase was blown dry by N_2, then dissolved in 1mL trichloromethane followed by filtering through 0.22 μm organic membrane. Finally, the degradation rate was measured by GC-MS, using chlorpyrifos as internal standard.

3. GC-MS analysis

The degradation of chlorpyrifos was analyzed by GC-MS. The chromatographic settings were: the injector was in a splitless mode; the injection port was at 260℃; sample volume was 1 μL; the carrier gas was helium at a pressure of 53.5 kPa and a flow-rate of 1.00 $mL \cdot min^{-1}$. The furnace temperature for chlorpyrifos solutions was initially at 40℃ for 1 min and then increased at a rate of 10℃ min^{-1} to 180℃, followed by 2 min stabilization, then increased at a rate of 30℃ min^{-1} to 290℃,

followed by 5 min stabilization. The mass spectrometer conditions were: ion source temperature was 300℃; interface temperature was 250℃; detector gain was in an absolute mode; detector voltage was at 1.0 kV; acquisition was in a SIM mode; scan interval was 0.2s; solvent cut was 3min. GC-MS solution software (release version 2.30) was used to identify and process the data.

Fig. S1 (A) TEM images of Ce-free bare CDs. (B) Size distribution of Ce-free bare CDs analyzed from multiple images.

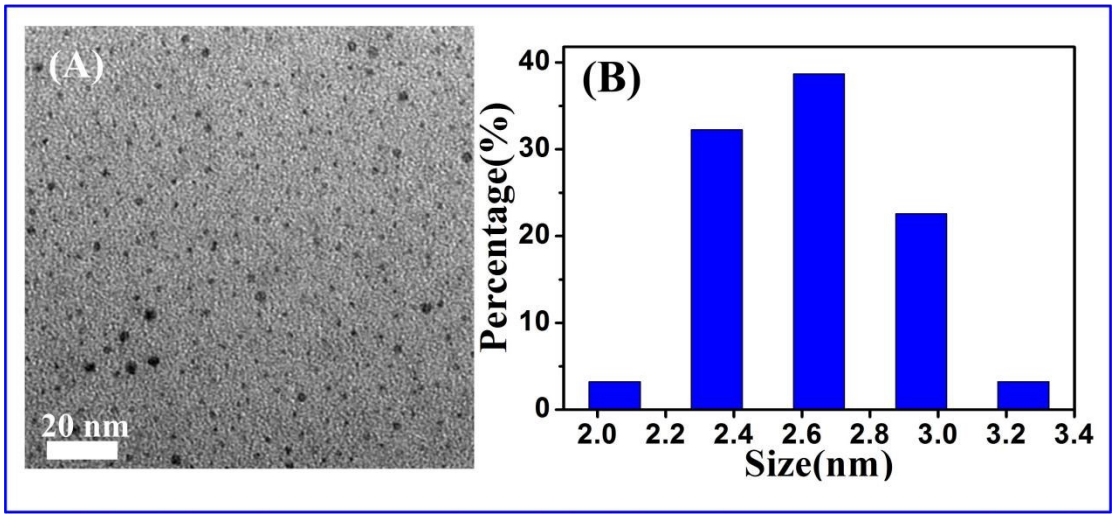

Fig. S2 (A) The absorption and (B) Fluorescence emission spectra of the Ce-free bare CDs.

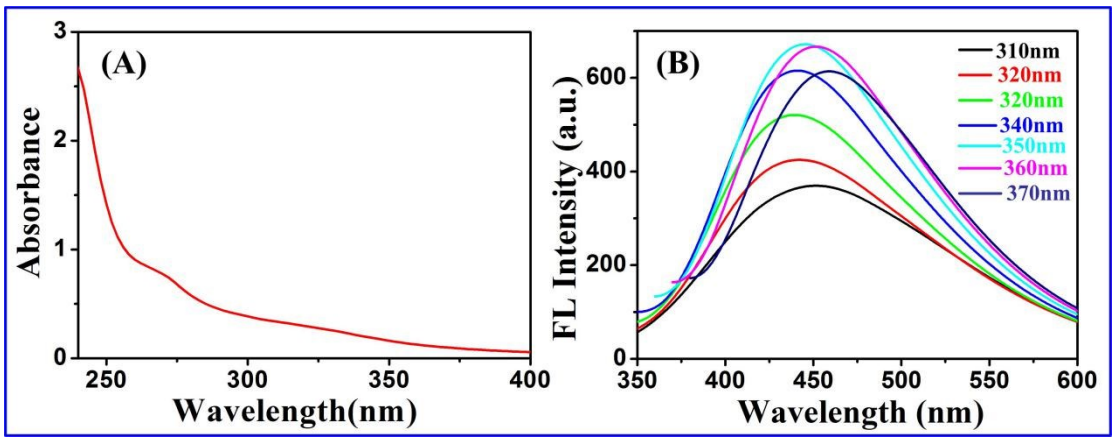

Fig. S3 EDS spectrum of the CeCDs.

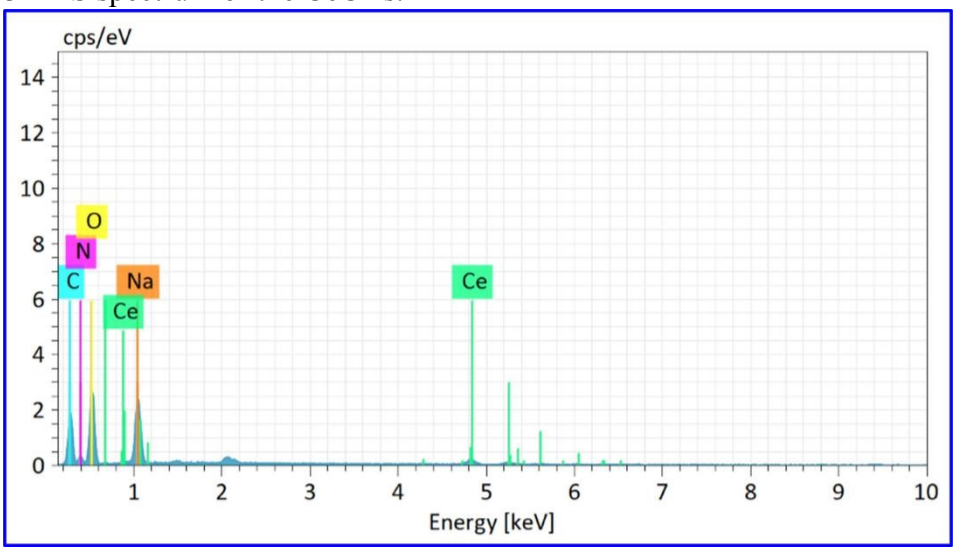

Fig. S4 Dependency of catalytic activity of CeCDs on synthetic conditions: (A) ratio of EDTA to cerium nitrate, (B) reaction temperature, (C) reaction time.

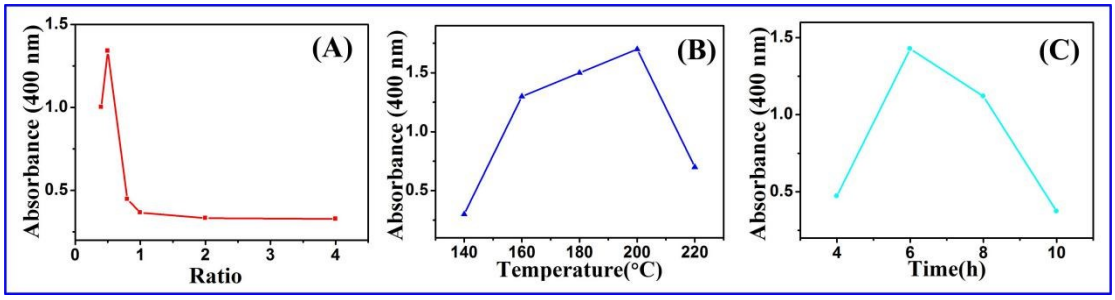

Fig. S5 The pH-dependent absorbance changes at 400 nm during the assay for phosphatase activity of the CeCDs.

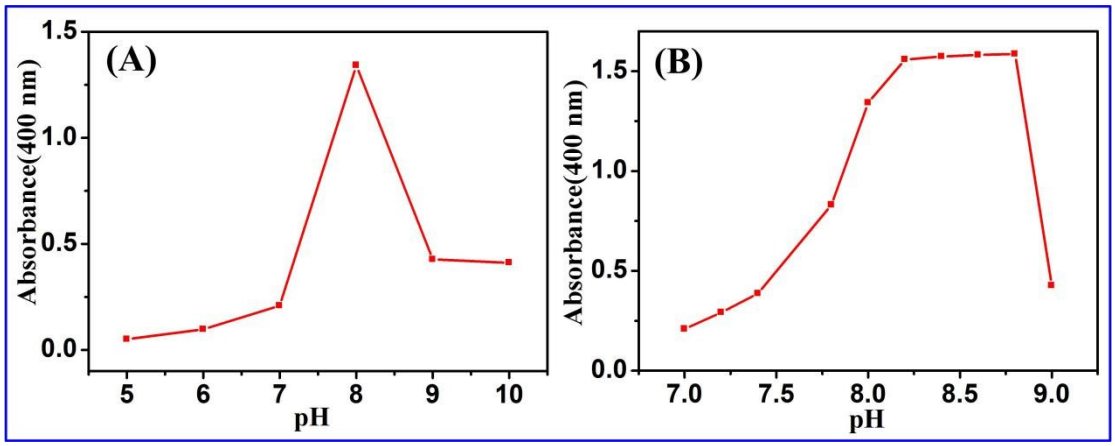

Fig. S6 (A) Time-dependent UV-vis spectral changes in catalytic hydrolysis of BNPP by free - Ce bare CDs. (B) Plot of absorbance at 400 nm versus time.

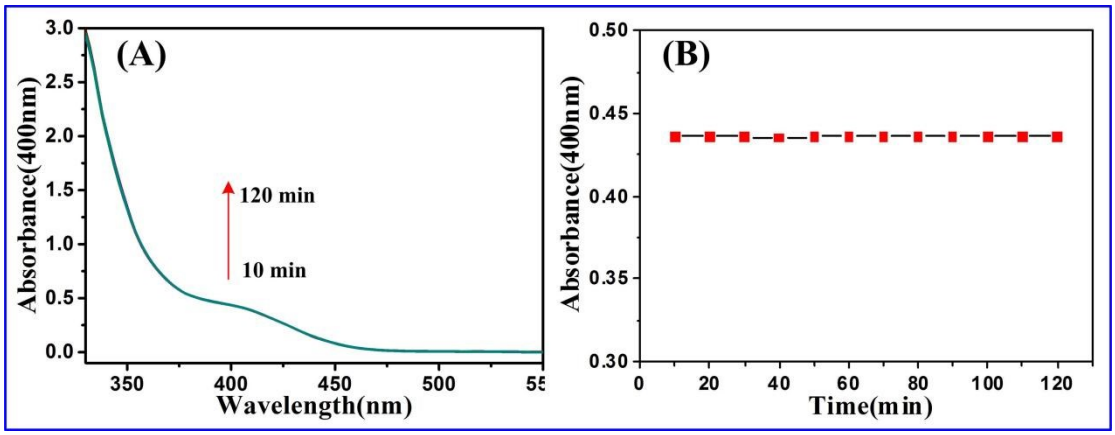

Fig. S7 (A) Time-dependent UV-vis spectral changes in the hydrolysis of BNPP catalyzed by the CeCDs under dark conditions. (B) Plots of $\log[A_\infty/(A_\infty-A_t)]$ versus time.

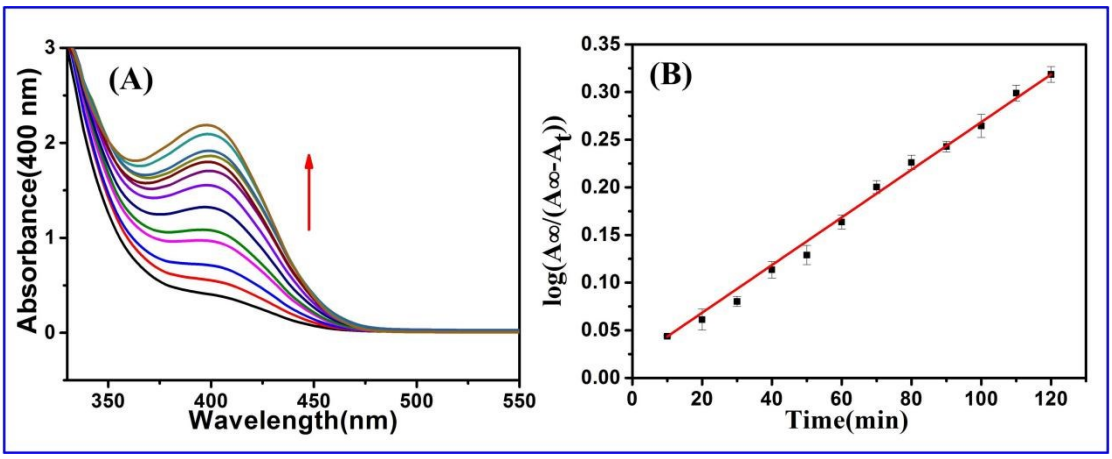

Fig. S8 (A) Time-dependent UV-vis spectral changes in BNPP solution catalyzed by CeCDs upon addition of potassium persulfate. The spectra were recorded at intervals of 10 min. (B) Plots of $\log[A_\infty/(A_\infty-A_t)]$ versus time t for the catalytic hydrolytic cleavage of BNPP in the presence of electron scavenging agent (potassium persulfate).

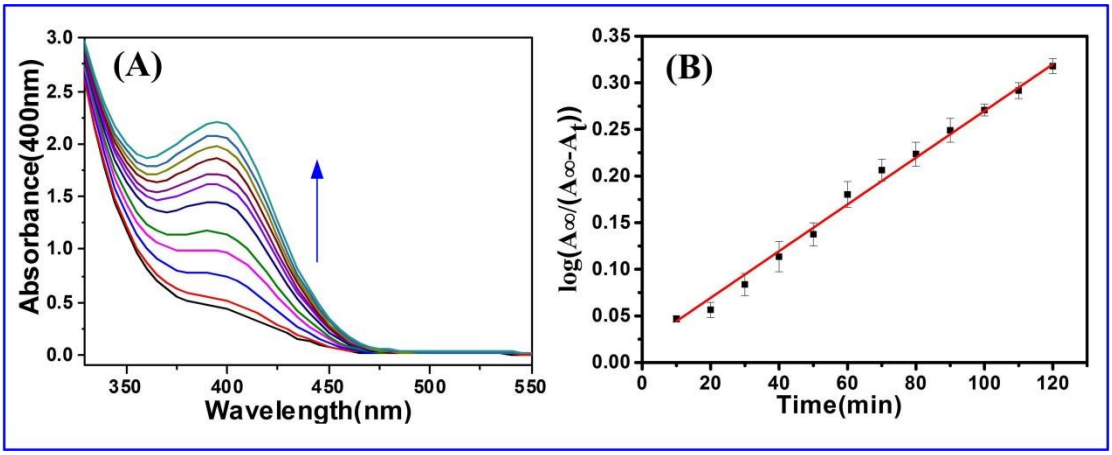

Fig. S9 Fluorescence spectra of the CeCDs with increasing amounts of BNPP at pH 8.5.

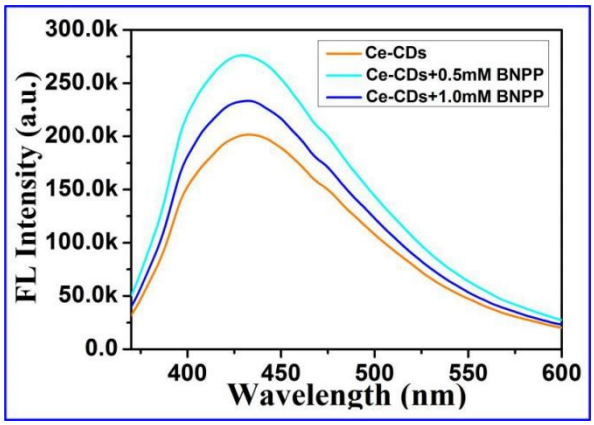

Fig. S10 (A) Chromatographic profiles of a standard solution of phosphate. (B) Chromatographic profiles of phosphate ion (the hydrolysis product of chlorpyrifos

catalyzed by the CeCDs).

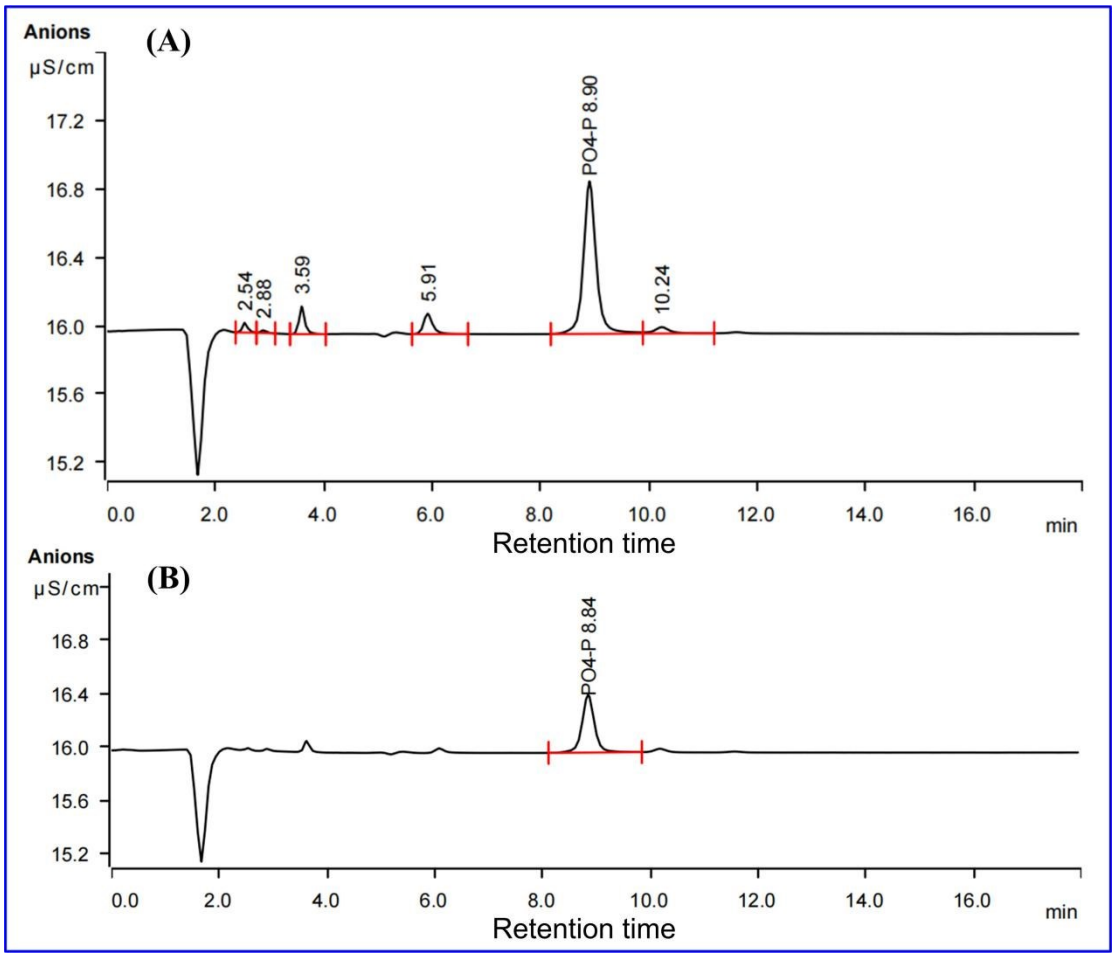

Fig. S11 Kinetic plot of (A) v vs S (B) 1/v vs 1/S for phosphatase activity where v = initial rate and [S] = [BNPP].

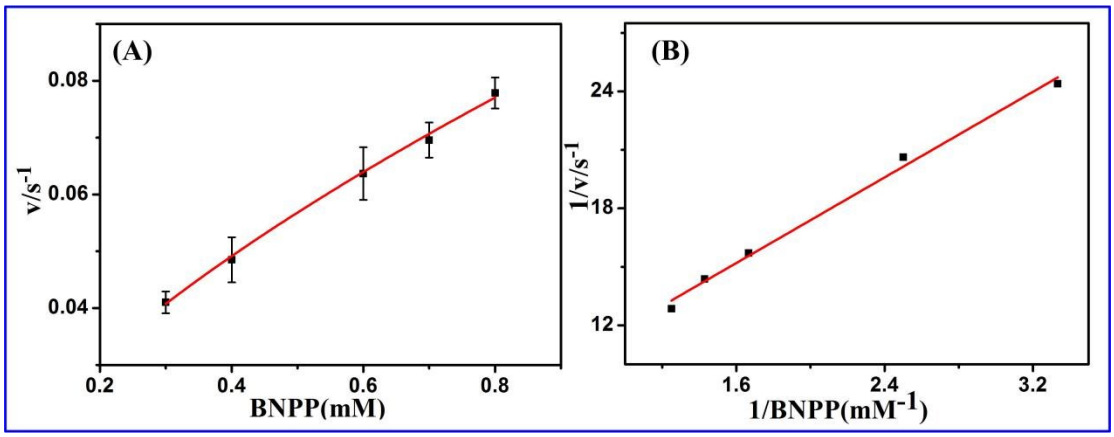

Fig. S12 (a) UV-vis absorption spectrum of p-nitrophenol, (b) Fluorescence emission spectrum of the CeCDs (λ_{ex} = 350 nm).

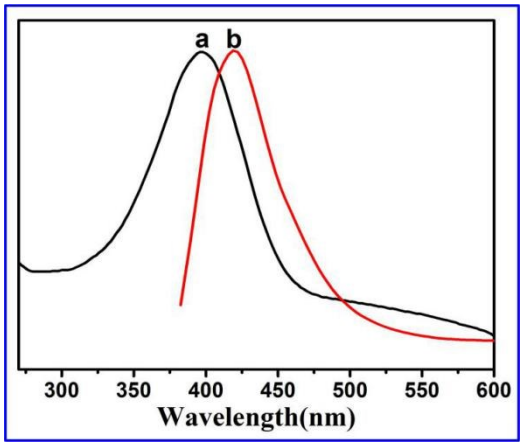

Fig. S13 Fluorescence decay profiles for the CeCDs in the absence and presence of BNNP.

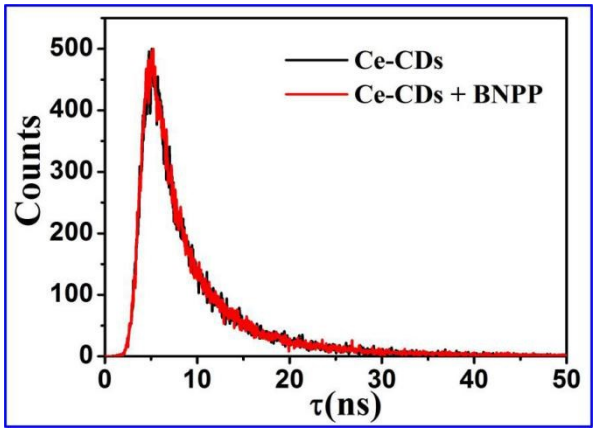

Fig. S14 Time-dependent GC-MS chromatogram of chlorpyrifos sample catalyzed by Ce-free bare CDs. Retention time: 19.91 min.

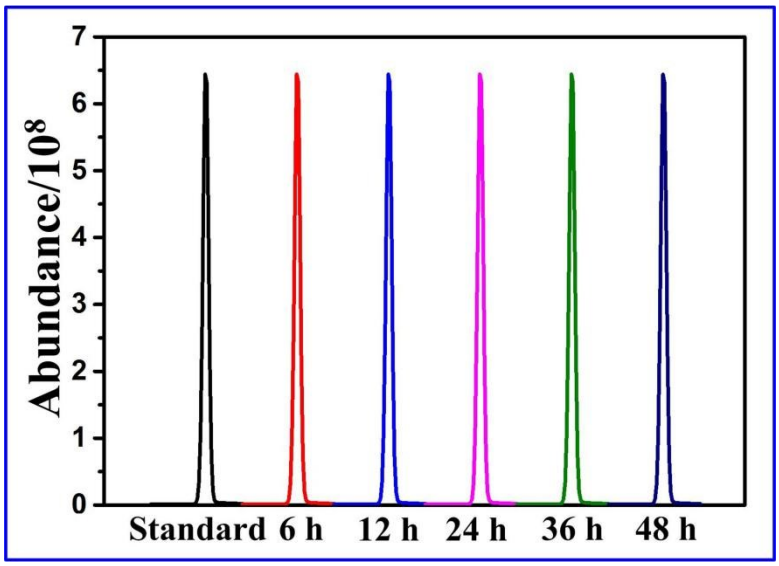

Table S1 Comparison of kinetic parameters for the catalytic hydrolytic cleavage of BNPP.

Catalyst	Vmax(M/s)	Km(M)	K(min^{-1})	Refs.
$[Fe_4(cpdp)_2(phth)_2(OH)_2]\cdot 8H_2O$	6.83×10^{-9}	4.80×10^{-3}	1.64×10^{-3}	[1]
$[Fe_4(cpdp)_2(terephth)_2(OH)_2]$	2.66×10^{-9}	4.08×10^{-3}	6.03×10^{-4}	[1]
$[Zn_4(Hcpdp)_2(suc)]Br_2\cdot 12H_2O$	7.64×10^{-10}	7.60×10^{-3}	1.83×10^{-4}	[1]
$[Zn(L^1)Cl_2](ClO_4)_2\cdot H_2O$	7.09×10^{-9}	2.08×10^{-3}	8.52×10^{-3}	[2]
$[Zn(L^2)Cl_2](ClO_4)2H_2O$	1.83×10^{-8}	6.99×10^{-4}	2.20×10^{-2}	[2]
$[Zn(bpy)Cl_2]\ 2H_2O$	2.37×10^{-10}	6.82×10^{-3}	3.28×10^{-5}	[2]
$[Cu(tacn)(OH_2)_2]^{2+}$	/	/	1.50×10^{-5}	[3]
Co_2L	4.62×10^{-4}	9.30×10^{-4}	/	[4]
$[Ni_2L(\mu\text{-}OH)]\ (ClO_4)_2$	/	/	8.94×10^{-3}	[5]
$[Fe^{II}{}_2LCl_3]\cdot 3H_2O$	3.10×10^{-9}	3.10×10^{-3}	3.12×10^{-3}	[6]
$[Zn^{II}{}_2(L_{-2H})(AcO)(H_2O)][Zn^{II}{}_2L']$	/	6.15×10^{-2}	2.76×10^{-4}	[7]
$[Zn^{II}{}_2(HL^1)(CH_3COO)]^+$	4.37×10^{-11}	1.96×10^{-3}	7.56×10^{-5}	[8]
CeCDs	1.58×10^{-4}	8.66×10^{-4}	2.00×10^{-3}	This work

Table S2 Degradation efficiency of chloryrifos catalyzed by the CeCDs.

Degradation time	Degradation percentage
6h	4.10%
12h	20.10%
24h	41.85%
36h	61.05%
48h	74.50%

References

1. Yan, F.; Zu, F.; Xu, J.; Zhou, X.; Bai, Z.; Ma, C.; Luo, Y.; Chen, L., Fluorescent carbon dots for ratiometric detection of curcumin and ferric ion based on inner filter effect, cell imaging and PVDF membrane fouling research of iron flocculants in wastewater treatment. *Sensors and Actuators B: Chemical* **2019,** *287*, 231-240.
2. He, J.; Sun, J.; Mao, Z.-W.; Ji, L.-N.; Sun, H., Phosphodiester hydrolysis and specific DNA binding and cleavage promoted by guanidinium-functionalized zinc complexes. *Journal of inorganic biochemistry* **2009,** *103*, 851-858.
3. Fry, F. H.; Fischmann, A. J.; Belousoff, M. J.; Spiccia, L.; Brügger, J., Kinetics and mechanism of hydrolysis of a model phosphate diester by [Cu (Me3tacn)(OH2) 2] 2+(Me3tacn= 1, 4, 7-trimethyl-1, 4, 7-triazacyclononane). *Inorganic chemistry* **2005,** *44*, 941-950.
4. Zhao, M.; Xue, S.-S.; Jiang, X.-Q.; Zheng, L.; Ji, L.-N.; Mao, Z.-W., Phosphate ester hydrolysis catalyzed by a dinuclear cobalt (II) complex equipped with intramolecular β-cyclodextrins. *Journal of Molecular Catalysis A: Chemical* **2015,** *396*, 346-352.
5. Sanyal, R.; Zhang, X.; Chakraborty, P.; Giri, S.; Chattopadhyay, S. K.; Zhao, C.; Das, D., Role of solvent in the phosphatase activity of a dinuclear nickel (II) complex of a Schiff base ligand: mechanistic interpretation by DFT studies. *New Journal of Chemistry* **2016,** *40*, 7388-7398.
6. Chen, X. Q.; Peng, X. J.; Wang, J. Y.; Wang, Y.; Wu, S.; Zhang, L. Z.; Wu, T.; Wu, Y. K., Efficient increase of DNA cleavage activity of a diiron (III) complex by a conjugating acridine group. *European Journal of Inorganic Chemistry* **2007,** *2007*, 5400-5407.
7. Chen, J.; Wang, X.; Zhu, Y.; Lin, J.; Yang, X.; Li, Y.; Lu, Y.; Guo, Z., An asymmetric dizinc phosphodiesterase model with phenolate and carboxylate bridges. *Inorganic chemistry* **2005,** *44*, 3422-3430.
8. Buchholz, R. R.; Etienne, M. E.; Dorgelo, A.; Mirams, R. E.; Smith, S. J.; Chow, S. Y.; Hanton, L. R.; Jameson, G. B.; Schenk, G.; Gahan, L. R., A structural and catalytic model for zinc phosphoesterases. *Dalton Transactions* **2008**, 6045-6054.